



HAL
open science

Shear-enhanced membrane filtration of model and real microalgae extracts for lipids recovery in biorefinery context

Liliana Villafaña-López, Erika Clavijo Rivera, Shuli Liu, Estelle Couallier, Matthieu Frappart

► To cite this version:

Liliana Villafaña-López, Erika Clavijo Rivera, Shuli Liu, Estelle Couallier, Matthieu Frappart. Shear-enhanced membrane filtration of model and real microalgae extracts for lipids recovery in biorefinery context. *Bioresource Technology*, 2019, 288, pp.121539. 10.1016/j.biortech.2019.121539 . hal-02319633

HAL Id: hal-02319633

<https://hal.science/hal-02319633>

Submitted on 18 Oct 2019

HAL is a multi-disciplinary open access archive for the deposit and dissemination of scientific research documents, whether they are published or not. The documents may come from teaching and research institutions in France or abroad, or from public or private research centers.

L'archive ouverte pluridisciplinaire **HAL**, est destinée au dépôt et à la diffusion de documents scientifiques de niveau recherche, publiés ou non, émanant des établissements d'enseignement et de recherche français ou étrangers, des laboratoires publics ou privés.

Shear-enhanced membrane filtration of model and real microalgae extracts for lipids recovery in biorefinery context

Liliana Villafaña-López^{a,b}, Erika Clavijo Rivera^a, Shuli Liu^{a,c}, Estelle Couallier^{a,*}, Matthieu Frappart^a

^aCNRS, GEPEA, Université de Nantes, 37 Boulevard de l'université, BP 406, 44602 Saint-Nazaire cedex, France

^bCIATEC A.C., Centro de Innovación Aplicada en Tecnologías Competitivas, Omega 201, Col. Industrial Delta, 37545 León, Gto., Mexico.

^cADEME, 20 avenue du Grésillé, BP90406, 49004 Angers cedex 01, France

Abstract

In this work, the hydrodynamic effects of rotating disk filtration (with maximum shear rates of $16\,000\text{ s}^{-1}$ and $66\,000\text{ s}^{-1}$) were evaluated and compared with the crossflow filtration ($16\,000\text{ s}^{-1}$) in the recovery of lipids from a model solution that simulates the characteristics of *Parachlorella kessleri* aqueous extracts. Four polymeric membranes were tested. The PAN 500 kDa membrane along with the rotating disk filtration presented the best performances for lipid concentration and coalescence. The rotating disk filtration was tested with real microalgae extracts, confirming the total lipid retention and the limited membrane fouling.

Keywords: Microalgae, Lipids, Rotating disk filtration, Ultrafiltration, Oil-in-water emulsion

*Corresponding author

Email address: estelle.couallier@univ-nantes.fr (Estelle Couallier)

1. Introduction

Satisfying the increasing world energy demand with renewable natural resources has significant environmental benefits, that are of great importance to both researchers and entrepreneurs alike. In this context, a very attractive area of research is the cultivation and harvest of microalgae for biodiesel production. A large variety of microalgae has been characterized with regard to cultivation conditions, biomass productivity, lipid content, and lipid productivity (Chun-Yen et al., 2011). Between the different varieties of microalgae, the *Parachlorella kessleri* species stand out for their high lipid production; in addition, the lipid production of this specific species has been successfully scaled to the semi-industrial level (Ota et al., 2016) with promising results. Several studies concerning the dilution of nutrient media (Li et al., 2013), variation of carbon sources (Hamza et al., 2013), and macronutrient limitation (Ota et al., 2016) have demonstrated that nitrogen limitation is (at the moment) the most widely used method to induce lipid overproduction (Li et al., 2013).

A crucial step in biodiesel production is the cell disruption and lipid extraction from the harvested cells. Since lipids are intracellular compounds, cell disruption is absolutely necessary to increase the amount of lipids recovered (Lee et al., 2012); the extraction efficiency, and the lipid integrity depend on the disruption processes being used (Byreddy et al., 2015). The disrupted microalgae form a mixture composed of the extracted lipids, among other intracellular components, cell debris, and solvent (Halim et al., 2012). The extraction of lipids directly from the wet disrupted microalgae cells reduces the required monetary and time investment associated with drying processes (’t Lam et al., 2018).

The filtration process is an attractive option for the lipid concentration from the wet disrupted cells because it can be automated, and it can treat large volumes (Kumar Patel et al., 2013). Additionally, filtration methods allow for a drastic reduction of the required solvents and chemicals used for extraction (Safi et al., 2014). Operating conditions and feed properties such as the transmembrane pressure (TMP), shear rate, membrane hydrophilicity, initial oil concentration, salinity, and pH all play an important role in membrane separation processes (Chakrabarty et al., 2008; Li et al., 2009). The main drawback of the filtration process is the membrane fouling due to the deposition of microalgae material on the

membrane surface and/or inside the membrane pores (Waghmare et al., 2016; Marcati et al., 2014; Kumar Patel et al., 2013). In recent years, shear-enhanced or dynamic filtration (DF) has emerged as an interesting option that reduces membrane fouling. This technique limits the cake growth at the membrane surface (Rios et al., 2011; Ding and Jaffrin, 2014) by increasing the shear rate. This increase can be produced by generating turbulence using a rotating disk over a fixed membrane, or by rotating (or vibrating) the membrane itself (Jaffrin, 2008).

Rotating disk (RD) is a type of DF module that provides high permeate fluxes at a steady shear rate, with good performance and low energy requirements (Moulai-Mostefa et al., 2007; Jaffrin et al., 2004; Hwang et al., 2016). The aforementioned characteristics make this process a very favorable option for biotechnological applications. For example, a vibrating DF system was used to concentrate lipids from steam exploded biomass by Lorente et al. (2017). A polyethersulfone (PES) membrane with a molecular weight cut off (MWCO) of 5 kDa, and a polyvinylidene fluoride membrane (PVDF, MWCO 100 kDa) were selected to perform the filtration at 5 bar. The flux reached 5 to 65 L h⁻¹ m⁻². However, even with the promising results that the RD filtration can provide towards lipid concentration from disrupted microalgae cells, its usage in microalgae biorefining has been generally left unexplored. If a methodology for carrying out lipid concentration from disrupted cells can be established using membrane technology, this process could be used for obtaining different microalgae fractions with minor modifications.

In this work, the performances of the RD technique applied towards the concentration of lipids from microalgae aqueous extracts were evaluated. A model solution (Clavijo et al., 2017) to test the different polymeric membranes was used due to limited access to large volumes of real microalgae culture. Moreover, the large variability inherent to the real products would have limited the comparisons. The membrane with the best separation characteristics was used to compare the performances between crossflow (CF) filtration and RD filtration. Finally the RD filtration was tested with real microalgae aqueous extracts and compared to the CF filtration of the same products.

2. Material and methods

2.1. Real microalgae extracts

The characteristics of the *Parachlorella kessleri* culture used in this work was grown in autotrophic starving conditions; two aqueous extracts containing dispersed lipids called supernatant (SN₁ and SN₂) were produced after bead milling and centrifugation of two different biomasses.

2.2. Model solution preparation

The model solution is an oil in water emulsion. It corresponds to the supernatant of a concentrated pretreated culture, after bead milling and separation of the cell fragments by centrifugation (Clavijo Rivera et al., 2018; Clavijo et al., 2017). It contains 2%_w of lipids in an aqueous phase (emulating a fresh water culture medium), with a pH of 7.4 and a conductivity equal to 790 μS cm⁻¹. The lipid phase contains 70%_w of neutral lipids coming from the mixture of vegetable oils and 30%_w of polar lipids constituted of commercial products. The emulsification was performed with a rotor-stator T-25 ULTRA-TURRAX (IKA). The aqueous phase was mixed with a polar lipid product (15%_w of the total lipid content) at 80 °C. The vegetable oils were mixed with a second polar lipid product (15%_w of the total lipid content) at 80 °C. The aqueous and the oil phases were then mixed (24 000 rpm by 30 min) and then, cooled to room temperature during 20 h with gently stirring at 700 rpm.

2.3. Filtration modules

The RD module used in this study is described in detail in Refs. (Bouzerar et al., 2000b) and (Bouzerar et al., 2000a). This RD module is equipped with a disk of 15 cm of diameter that rotates inside a cylindrical housing. This disk has eight vanes that are each 2 mm wide by 6 mm tall. The disk can rotate at a maximum speed of 3000 rpm. The pressure is adjusted by operating a valve on the retentate outlet tubing. The peripheral pressure is measured at the top of the cylindrical housing by a pressure sensor. On the cover of the cylindrical housing (in front of the disk), a single circular membrane with dimensions of 8.4 cm of outer radius and 1.2 cm of inner

radius (usable area of 185 cm²) can be placed. Fig. 1a presents a cross-sectional view of the module design and its internal circulation path.

The movement of the disk near the fixed circular membrane creates a maximum shear rate ($\dot{\gamma}_{max}$) with turbulent flow, which is calculated as (Bouzerar et al., 2000a; Frappart et al., 2011),

$$\dot{\gamma}_{max} = 0.0296 \cdot \nu^{-\frac{4}{5}} \cdot (k\omega)^{\frac{9}{5}} \cdot R_d^{\frac{8}{5}}, \quad (1)$$

where ν is the kinematic viscosity (m²s⁻¹), k is the velocity factor, ω is the angular disk velocity (rad s⁻¹), and R_d is the disk radius (m). $k\omega$ is the angular velocity of the inviscid fluid.

The CF module is a Rayflow X100 (Orelis-Novasep). This module consists of two restraining plates that can contain up to two flat rectangular membranes, each with a usable area of 130 cm². Filtration pressure is adjusted with a valve, with one pressure sensor placed at the module inlet and another at the retentate outlet. Fig. 1b presents a schematic representation of this module. The maximum shear rate from the laminar flow on the membrane can be calculated as (Delaunay et al., 2008),

$$\dot{\gamma}_{max} = \frac{4}{e} \cdot v_{max}, \quad (2)$$

where $e = 0.5$ mm is the chamber thickness, and v_{max} is the tangential flow velocity obtained in the chamber (m s⁻¹). The experimental setup used in this study (the RD and the CF modules) is described in Ref. (Frappart et al., 2011). Table 1 shows the corresponding v_{max} and $\dot{\gamma}_{max}$ for the three different setups tested in this work.

2.4. Membranes

Four commercial membranes were selected. These membranes were manufactured by Orelis Environnement (Pleiade range), with differing polymer composition, hydrophilicity, and MWCO. The membranes used were a PES (200 kDa), a polyacrylonitrile (PAN 500 kDa), a PVDF (0.4 μ m), and another PVDF (1.5 μ m). Before being used, each membrane was cut, washed, and compacted in order to eliminate membrane preservatives (glycerol), and to ensure a steady water flux. The cleaning procedure involved the membrane rinsing with ethanol and demineralized

water; then, the membrane was submerged for 30 min in demineralized water (refreshed every 10 min). The experimental flux values were adjusted to 30 °C using a correction coefficient related to water viscosity (μ).

2.5. Screening of the membranes with the model solution

The permeate flux (J) variation versus the TMP was determined by recirculating the emulsion in a closed system at 30 °C. J was measured for the lowest TMP possible, then the permeate was returned to the feed tank and the TMP was increased with 0.1 bar steps, repeating the same procedure. Once the limiting flux was reached, two additional measurements were performed in order to verify the flux plateau.

2.5.1. Concentration experiment

The concentration experiment was evaluated through the volume reduction ratio (VRR). The emulsion was recirculated at 30 °C, collecting the permeate and returning the retentate back to the feed tank until reaching different VRR. In a batch system concentration, the VRR is defined as,

$$\text{VRR} = \frac{V_0}{V_f}, \quad (3)$$

where V_0 and V_f are the initial and final emulsion volumes. Samples of instantaneous retentate, permeate, and collected permeate were taken at each of these points. During this experiment the membrane performance was followed through the flux decline, membrane selectivity and total oil mass accumulated on the membrane. Flux decline was calculated as a function of the emulsion permeate flux (J) and the initial membrane demineralized water flux (J_w) according to the following expression,

$$\% \text{ Flux decline} = \left(1 - \frac{J}{J_w} \right) \times 100. \quad (4)$$

The membrane selectivity was verified through the retention rate (% R), which is a function of the permeate (C_p) and retentate (C_r) concentrations,

$$\% \text{ R} = \left(1 - \frac{C_p}{C_r} \right) \times 100. \quad (5)$$

The total oil mass accumulated on the membrane and non-membrane interfaces during the concentration experiment ($m_{\text{VRR}}^{\text{Tot}}$) was calculated as

$$m_{\text{VRR}}^{\text{Tot}} = (X_0 M_0) - (X_r M_r) - (X_p M_p) - \sum_{i=0}^n (X_r m_r^i + X_p m_p^i), \quad (6)$$

where X_0 , X_r , and X_p are the initial, retentate, and permeate mass fractions of oil in the emulsion ($g_{\text{oil}}/g_{\text{emulsion}}$), respectively. Likewise, M_0 , M_r , and M_p are the equivalent emulsion masses (g). m_r^i , and m_p^i are the samples mass (g) taken out of the system for each analysis, and i represents the sample taken out of the system from a total n number of samples. The amount of salt contained in the buffer that was used to prepare the emulsion, was subtracted from the different samples before calculating $m_{\text{VRR}}^{\text{Tot}}$.

The maximum amount of oil accumulated on the non-membrane interfaces of the RD module was obtained by recirculating the model solution trough the system for 7 h, without a membrane in order to reach equilibrium. A sample was taken at each hour of the experiment, and the oil content was quantified by gravimetric analysis. The maximum amount of oil accumulated at the non-membrane interfaces of the RD module was subtracted from Eq. (6). The final amount was divided by the apparent surface area of the membrane (m^2), obtaining the quantity of oil accumulated only on the membrane ($q_{\text{VRR}}^{\text{mb}}$) as,

$$q_{\text{VRR}}^{\text{mb}} = \frac{(m_{\text{VRR}}^{\text{Tot}} - m^{\text{non-membrane}})}{A}. \quad (7)$$

2.5.2. Cleaning procedure

The emulsion elimination from the membrane was performed right after the concentration experiment, once the remaining emulsion was expelled out of the filtration module. The cleaning procedure encompasses a cycle of three steps. First, recirculation of demineralized water (40 °C and 1.0 m s^{-1}) for 30 min; second, recirculation of sodium dodecyl sulfate (SDS, 8 mM, 40 °C) for 30 min, and ethanol (25 % in volume) for 60 min; and third, measurement of the demineralized water permeability adjusted at 30 °C. For membranes used with the real microalgae extract, another cleaning step was implemented using a commercial alkaline Ultrasil 110 (Ecolab) solution.

A long rinsing with water was performed after each step. The cleanability of the membrane was evaluated using the flux recovery ratio (% FRR) which relates the permeate flux after the cleaning procedure (J_r) and J_w as,

$$\% \text{ FRR} = \left(\frac{J_r}{J_w} \right) \times 100. \quad (8)$$

The membrane was considered clean when the % FRR was greater than 90 %.

2.6. Gravimetric analysis

The IR-30 Moisture Analyzer (Denver Instrument) was used to determine the emulsion dry matter, and therefore calculate the mass balance. This device is based on heating the sample with infrared light then determining the remaining amount of dry mass. A measuring accuracy of 0.05 g is reported for an initial sample weight from 5 g to 10 g. Glass fiber pads were used to evenly spread the samples. Prior to the sample analysis, a glass fiber pad and a weighing dish of 90 mm in diameter were dried at 105 °C for 5 min, eliminating any trace of moisture. The samples were dried at 105 °C and automatic drying time. To ensure accuracy all samples were replicated three times.

2.7. Droplet size distribution

The droplet size distribution (DSD) of the emulsion was determined with a Mastersizer 3000 laser diffraction particle size analyzer (Malvern). This instrument is equipped with the hydro large volume and small volume wet dispersion units. The device has a detection particle size range of 0.01 μm to 3500 μm . The samples were analyzed (in triplicate) without dilution, using a refraction index of 1.44 and a absorption index of 0.003.

2.8. Ultrapure water contact angle

The ultrapure water contact angle (θ_w) quantifies the wettability of a solid surface. The water used has a resistivity of 15 $\text{M}\Omega\text{cm}$ and $\text{pH}=8.35 \pm 0.49$ at 25 °C. θ_w was measured on the four clean and emulsion-fouled membranes. The Drop Shape Analyzer – DSA30A TRACKER instrument

was used for this purpose in sessile drop mode. Before the θ_w measurement, the fouled membranes were removed from the filtration modules immediately after the concentration experiment in order to maintain the fouled surface. The membrane surface was then gently rinsed with demineralized water to eliminate the excess emulsion. Both membrane samples were dried in an oven for 48 h at 35 °C, followed by 24 h in a desiccator. The membranes were then fastened on glass slides using double-sided tape.

The water drops were dosed using a glass syringe (500 μL) with a disposable stainless steel needle (diameter of 0.5 mm). The approximate volume of each drop was 2.5 μL . θ_w was measured 100 ms after drop deposition. The left and right contact angles of each drop were calculated from the digitized image using the DSA software. The profile of the sessile drop was calculated using a tangent method that fits the drop to a general conic equation. The derivative of the equation at the drop baseline is the slope at the three-phase contact point, which is used to determine the contact angle. 12 droplets of the water were deposited on different sections of the same membrane sample, increasing the accuracy of the average value of the contact angle. This technique presents an accuracy of 2° to 5.5° (Diagne et al., 2013).

3. Results and Discussion

3.1. Screening evaluation of the membranes with the model solution

3.1.1. Determination of the critical pressure

The limiting flux (J_{lim}) is the maximum steady flux achieved by increasing the TMP (Hurt et al., 2015); the TMP value at which this occurs is defined as the maximum pressure (P_{max}). The critical flux (J_c) can be generally defined as the first permeate flux at which a prominent fouling takes place (Hurt et al., 2015), and the corresponding pressure for this flux is called the critical pressure (P_c). This P_c corresponds to the TMP at which the normalized flux (J/J_w) begins to decrease, which indicates an increase in membrane fouling. Figs. 2a and 2b feature the average variation of the permeate flux (J), and J/J_w as functions of the TMP taken at 30 °C for the

PAN 500 kDa and PVDF 0.4 μm membranes. The initial J_w was measured and adjusted at 30 $^\circ\text{C}$.

As can be seen in Fig. 2a, the 0.4 μm PVDF membrane presents a J which increases with the TMP; for this membrane, a value of $J_{\text{lim}} = 66 \pm 1$ $\text{L h}^{-1} \text{m}^{-2}$ occurs at $P_{\text{max}} = 0.6$ bar. For the PAN membrane, J_{lim} never reaches a steady value in the range of TMP studied in this work; therefore, P_{max} can not be determined. Different fouling behavior of the membranes with similar filtration conditions can be explained considering their pore size distribution and degree of hydrophilicity; these characteristics determine the water and oil droplet permeation. Membrane polarization, attraction/adsorption between the membrane and the oil droplets, oil layer formation at the membrane surface, and the steric effect all play a role in determining the oil droplet retention by the membrane.

Fig. 2b shows that the initial J/J_w is close to 1.0 for both membranes. This indicates that the permeate flux is nearly the same as the water flux at low TMP, indicating that fouling is very low. However, the P_c of the 0.4 μm PVDF membrane was detected around 0.4 bar; for the 500 kDa PAN membrane, P_c was between 0.5 and 0.6 bar. For $\text{TMP} > P_c$, the J/J_w begins to decrease inversely proportional to the TMP for both membranes, indicating that the membrane fouling has begun. The 500 kDa PAN membrane has a slow, gradual decrease, while the 0.4 μm PVDF membrane has a significantly steeper decline. Table 2 presents the average J_w at 1 bar, the J_{lim} , J_c along with their variability (σ), P_{max} , and P_c values of the different membranes used in this study. The initial water contact angle (θ_w^0) of the different membranes was measured following the procedure described in Sec. 2.8. Materials with $\theta_w < 45^\circ$ are highly-hydrophilic, when $45^\circ < \theta_w < 90^\circ$, they have both hydrophilic/hydrophobic properties, and for $\theta_w > 90^\circ$, the materials are hydrophobic (Świerczyńska et al., 2016).

The 500 kDa PAN membrane presented relatively high P_c values along with the lowest θ_w^0 value (75.0 ± 2.4). This suggest a high degree of membrane hydrophilicity that might limit fouling formation. The 1.5 μm PVDF membrane also presented relatively high P_c values despite its θ_w^0 value (82.3 ± 0.7), which indicates hydrophilic/hydrophobic membrane properties. Therefore, the potential accumulation of lipids on the membrane did not have a significant impact on the water permeation and the critical pressure because of the large pore size, that allowed the permeation of water but

also some fine oil droplets. During the screening evaluation the 1.5 μm PVDF membrane presented turbid permeates, while transparent permeates were obtained for the remainder of the membranes. 200 kDa PES and 0.4 μm PVDF membranes presented the lowest P_c values; therefore, a considerably high membrane fouling was supposed for both cases. For the former membrane, this fouling was mainly due to its small MWCO leading to a high lipids retention and probable adsorption pore blocking or cake formation. In the latter membrane, the fouling was due to its hydrophobic properties ($\theta_w^0 = 95.1 \pm 1.2$) thus a strong adsorption.

3.1.2. Concentration experiment

The concentration experiment was carried out just after the critical pressure measurement. The TMP of the concentration experiment was 90 % of the P_c ; this percentage was selected in order to have the highest permeate flux while avoiding strong membrane fouling. The examples of the evolution of J and its normalized representation versus the VRR during the concentration experiments for the 500 kDa PAN and 0.4 μm PVDF membranes are presented in Fig. 3.

J and J/J_w decreased with the VRR; this behavior is similar for all the membranes studied in this work. The 500 kDa PAN and 0.4 μm PVDF membrane presented an initial J/J_w around 0.9 and 0.7, respectively. At the highest VRR the normalized flux decreased 22 % for the former membrane, and 14 % for the latter membrane. Table 3 shows the % Flux decline, % FRR, $q_{\text{VRR}}^{\text{mb}}$, θ_w^0 , and water contact angle after the concentration experiment (θ_w^{VRR}) for all membranes at an average VRR = 4.3 ± 0.1 .

As already observed during previous critical pressure measurements, concentration experiments do not modify the retention behavior of the membrane. Oil retention was higher than 95 % for each membrane. An increased hydrophilicity (lower θ_w^{VRR} value) in comparison with the clean membranes (θ_w^0) was observed for all the membranes. The 200 kDa PES membrane presented a very high % Flux decline along with the lowest % FRR. This suggests a high degree of membrane fouling that is difficult to remove which has a significant impact on the membrane properties. In fact, this membrane presented the greatest increase in hydrophilicity, 28 % that might be due to the adsorption of the polar lipids present in the model solution formulation. These results suggest that the oil droplet

accumulation on the membrane is responsible for the strong fouling of the membrane.

The 500 kDa PAN membrane presented a low value of % Flux decline, and a total % FRR. This membrane behavior suggests the formation of a fouling layer that is easily removed. In fact, a large amount of the oil droplets accumulated on the membrane surface were almost completely eliminated when gently rinsed before the measurement of θ_w . The hydrophilic properties of the fouling may also be near from the membrane properties. This led to a very small increase in the membrane hydrophilicity of only 8 %. The large quantity of accumulated matter had a low impact on the filtration performances. This indicates a different structure of the fouling.

The 0.4 μm PVDF membrane presented a % Flux decline between 42 and 45 %, and a % FRR < 90 % that suggests an irreversible membrane fouling. This membrane presented the highest amount of accumulated oil and an increased hydrophilicity of 11 %; this membrane changed from hydrophobic to hydrophilic due to the accumulation of polar lipids. This performance indicated a strong fouling, which was expected due to the initial hydrophobic properties and MWCO of the membrane that led to pore blocking and cake formation.

The 1.5 μm PVDF membrane presented a % Flux decline between 23 % to 85 %, along with a % FRR < 90 %. The lowest quantity of oil accumulated was calculated for this membrane. A turbid permeate was observed for the PVDF 1.5 μm membrane. Because of the MWCO of the membrane, some oil droplets could be accumulated in the pores reducing their size and provoking a fast, irreversible, and internal membrane fouling (pore blocking and pore constriction). A small amount of polar lipids were present on the membrane surface, leading to an increase in the hydrophilicity of only 2 %.

Considering all the previous results, the membrane that presented the best oil separation performances was the 500 kDa PAN membrane. This membrane had a high range of P_c , and the highest initial hydrophilicity level amongst the membranes included in this study. During the concentration experiment, it presented complete oil retention, the lowest % Flux decline, and was the only one with a % FRR > 90 %. Also, the oil accumulated on the membrane (polar lipids) improved the hydrophilicity. In addition to these experimental observations, other works have demonstrated that this type of membrane (in both crossflow and dynamic

filtration modules) is well suited for microalgae suspensions, as it presents less adsorption of cells or cellular compounds (Rossi et al., 2004; Rossignol et al., 1999; Frappart et al., 2011). The same membranes were tested using the crossflow filtration technique, confirming the classification of the membranes with respect to the flux decline described above (Clavijo et al., 2017).

3.2. Influence of the hydrodynamics on the filtration of the model solution

The hydrodynamic impact on the filtration performance was studied using the CF and RD modules along with the previously selected 500 kDa PAN membrane. Three different setups were tested in this work and are shown Table 4. The permeate flux measurements versus the TMP were carried out as described in Sec. 2.5 for the CF filtration and RD filtration at 365 rpm. The results collected were compared with the best result obtained for the RD filtration at 800 rpm, described in the previous section. J_{lim} , P_{max} , J_c , and P_c values for the three different setups are also presented in Table 4.

For both RD speeds, J never reached a steady value in the range of TMP studied in this work, therefore J_{lim} and P_{max} could not be measured. Only the CF filtration presented J_{lim} and P_{max} values. It can be seen that P_c increased with the v_{max} . The concentration experiments were carried out just after the P_c determination, as described in Sec. 3.1.2. The TMP of the concentration experiment was 90% of the P_c . The three setups presented a similar J evolution having an average value of $28 \pm 16 \text{ m s}^{-1}$ at a VRR = 1; after this, J began to decrease with the VRR. Fig. 4 shows the evolution of the normalized J/J_w versus the VRR with the 500 kDa PAN membrane during the CF and the RD filtrations.

Membrane fouling can be limited by high shear rates (Zhao et al., 2016; Zhang and Ding, 2015; Goh et al., 2018); therefore, the smallest decrease in the J/J_w ratio was expected for the RD filtration at 800 rpm since the $\dot{\gamma}_{\text{max}}$ was more than four times larger than the CF filtration and the RD filtration at 365 rpm. On the other hand, the CF filtration and the RD filtration at 365 rpm had the same $\dot{\gamma}_{\text{max}}$ value; however, the CF filtration presented a laminar regime while the RD filtration had a turbulent one. This turbulent flow can more efficiently enhance the convection of particles away from the membrane (Frappart et al., 2011; Du et al., 2017; Zhang and Ding, 2015; Abid et al., 2017; Goh et al., 2018). As can be seen in Fig. 4,

the J/J_w ratio decreased progressively with the VRR for the three different setups. Table 5 presents % Flux decline and $q_{\text{VRR}}^{\text{mb}}$ measured during the concentration experiment at a $\text{VRR} = 3.8 \pm 0.3$.

The retention rate and the cleanability were higher than 97% and 90%, respectively, for all experiments; the latter suggests a totally reversible membrane fouling. The CF filtration presented the highest $q_{\text{VRR}}^{\text{mb}}$ indicating the presence of a strong fouling on the membrane. As mentioned above, this low performance of the CF filtration can be explained by its laminar regime which allows a large accumulation of droplets on the membrane. The RD filtration at 365 rpm led to a $q_{\text{VRR}}^{\text{mb}}$ value lower than at 800 rpm but the same flux decline. This may be due to different fouling mechanisms.

3.2.1. Effect on the hydrodynamics on the DSD

The applied pressure in the system has a huge impact on the oil droplets (Hong et al., 2003). In particular, coalescence is the joining of two or more (micron and submicron) oil droplets to form a single droplet with a larger diameter than the original (Chakrabarty et al., 2008). The effect of the CF filtration and the RD filtration on the coalescence or division of the oil droplets during the emulsion filtration was followed using the technique described in Sec. 2.7. The droplet size can be represented as a differential distribution, which represents the frequency of each size. The mode is the most repeated droplet diameter and corresponds to the highest point of the differential curve (Flügel, 2010). The evolution of the retentate volume DSD as a function of the VRR is shown in Fig. 5. It was not possible to measure the DSD in the permeates because of the low concentration of oil droplets.

The DSD presented a multimodal distribution, but the DSD during CF filtration changed the least. The major mode diameter during the CF filtration was maintained around $1.28 \pm 0.01 \mu\text{m}$. The major mode diameter during the RD filtration at 365 rpm increased with the VRR from 1.59 to $3.93 \mu\text{m}$. The volume fraction of the droplets with a diameter around $1.5 \mu\text{m}$ decreased and the volume fraction of the droplets with a diameter above $4 \mu\text{m}$ increased with VRR, indicating coalescence. On the contrary, during the RD filtration at 800 rpm the droplets with a diameter around $15 \mu\text{m}$ disappeared, indicating droplet division. The differences in the two DSD from the RD filtration were due to the different shear rate applied near the membrane. It is possible that the shear rate at 365 rpm

($16\,000\text{ s}^{-1}$), facilitated the oil droplet coalescence, while the higher shear rate at 800 rpm ($66\,000\text{ s}^{-1}$) divided the oil droplets. The laminar flow during CF filtration did not significantly affect the DSD.

The RD filtration offered better performances over the CF filtration because it limited membrane fouling, thus achieving relatively high ranges of P_c and permeation flux. During the concentration experiment, this RD filtration presented an almost complete retention of lipids and a full cleanability. However, oil droplet coalescence seemed to be favored at 365 rpm, while droplet breakage tended to occur at 800 rpm. This may have an impact on the fouling mechanisms. These results confirm former studies which demonstrated that the RD filtration presents increased performances compared to the CF filtration when applied to microalgae fractionation (Frappart et al., 2011; Lorente et al., 2017).

3.3. Filtration of real microalgae extract

Two *Parachlorella kessleri* cultures (1 g L^{-1}) were used to produce two batches of clarified supernatant, SN₁ and SN₂, dedicated to filtration tests at the pilot scale. The supernatants were filtered using the RD module equipped with a 500 kDa PAN membrane at 800 rpm. The composition of the supernatants, retentates (RET₁ and RET₂) and permeates (PERM₁ and PERM₂) are described in Table 6. The variations between SN₁ and SN₂ are due to differences in biomass and pretreatment (Liu et al., 2018).

After critical pressure measurements, the chosen TMP (90 % of the P_c) were 0.4 bar and 0.7 bar for SN₁ and SN₂, respectively. The normalized representation of the permeate flux of SN₁, SN₂, and model solution versus the VRR with the 500 kDa PAN membrane in the RD module ($\dot{\gamma}_{\max}=66\,000\text{ s}^{-1}$) and CF module ($\dot{\gamma}_{\max}=16\,000\text{ s}^{-1}$) are presented in Fig. 6. The J/J_w ratio was used for comparison due to the inherent variability of the individual membrane pieces.

The flux from the RD filtration with the supernatants was two times (SN₁) or three times (SN₂) superior to the water flux, which was not the case of the model solution. This means that during the filtration of the supernatants, the membrane permeability and hydrophilicity were strongly enhanced. Additionally, minimal membrane fouling was observed, thus reducing the needed time to reach the highest VRR. These changes in the

membrane properties may be due to the adsorption of some of the polar compounds (possibly proteins or polar lipids) present in the supernatants. Therefore, the calculation of the membrane cleanability was not realistic under such conditions. The J/J_w values in both cases are higher than those presented by Lorente et al. (2017) ($J/J_w < 0.2$). Their choice of the TMP (5 bar, probably above the P_c) coupled with a shear rate that may induce droplets division, and the membrane nature (PES or PVDF), have probably limited the flux performance. These results demonstrate the crucial choice of the filtration operating conditions.

The particle size distribution of the supernatants show that the particle diameter decreases very slightly, without significant changes (not shown). The retention rates of lipids, proteins, polysaccharides, and salts were calculated for the RD filtration at VRR=2. For both supernatants the lipids are totally retained, while the salts have a retention rate between 11 % and 15 %. The retention rates of proteins for SN₁ is 100 %, while for the SN₂ is 78 %. The polysaccharides are retained 48 % for SN₁ and 52 % for SN₂. These percentages depend on the supernatant and the pretreatment steps. They are not far from the retention rates obtained in CF filtration. Finally, the RD and CF filtrations of supernatants were compared confirming that the RD filtration presents better flux and J/J_w performance than the CF filtration.

4. Conclusions

This study first evaluated different commercial membranes, filtration regimes, and shear rates using an emulsion that simulates the characteristics of real microalgae extracts. The 500 kDa PAN membrane presented the best performances (oil retention, water permeation and cleanability) and the RD filtration offered better performances than the CF filtration. The performance of the RD module was then evaluated with real microalgae extracts, confirming those results. The importance of the operating conditions was demonstrated. Further investigation will allow finding the best pretreatment and filtration coupling for lipids and hydrophilic compounds separation.

Supplementary Material for this work can be found with the online version of the paper. It includes the preparation and characteristics of the

Parachlorella kessleri culture used in this work and the parameters (TMP, fluxes and permeabilities) registered during the filtration of real supernatants.

Acknowledgments

The authors gratefully acknowledge partial financial support from CONACYT-Mexico Grant No. 262944. This work was also funded by CNRS, France (interdisciplinary project Algues-Molécules-Territoire, 2014-2017), GIS Europôle Mer, France (Sciences et Ingénieries Marines, 2016-2017), and ADEME. The authors would also like to thank Guillaume Roelens, Delphine Drouin (GEPEA), Marie Cueff, Jordan Tallec (GEPEA, Algosolis) and Laurence Lavenant (INRA BIA) for their active participation in the preparation of the microalgae extracts and their analysis.

References

1. Abid, H. S., Johnson, D. J., Hashaikeh, R., Hilal, N., 2017. A review of efforts to reduce membrane fouling by control of feed spacer characteristics. *Desalination* 420 (Supplement C), 384 – 402.
URL <http://www.sciencedirect.com/science/article/pii/S0011916417313206>
2. Bouzerar, R., Ding, L., Jaffrin, M. Y., 2000a. Local permeate flux/shear/pressure relationships in a rotating disk microfiltration module: implications for global performance. *J. Memb. Sci.* 170 (1), 127 – 141.
URL <http://www.sciencedirect.com/science/article/pii/S0376738899003488>
3. Bouzerar, R., Jaffrin, M. Y., Ding, L., Paullier, P., 2000b. Influence of geometry and angular velocity on performance of a rotating disk filter. *AIChE Journal* 46 (2), 257–265
4. Byreddy, A. R., Gupta, A., Barrow, C. J., Puri, M., 2015. Comparison of cell disruption methods for improving lipid extraction from thraustochytrid strains. *Mar. Drugs* 13 (8), 5111.
URL <http://www.mdpi.com/1660-3397/13/8/5111>
5. Chakrabarty, B., Ghoshal, A., Purkait, M., 2008. Ultrafiltration of stable oil-in-water emulsion by polysulfone membrane. *J. Memb. Sci.* 325 (1), 427 – 437.
URL <http://www.sciencedirect.com/science/article/pii/S037673880800762X>
6. Chun-Yen, C., Kuei-Ling, Y., Rifka, A., Duu-Jong, L., Jo-Shu, C., 2011. Cultivation, photobioreactor design and harvesting of microalgae for biodiesel production: A critical review. *Bioresour. Technol.* 102 (1), 71 – 81, special Issue: Biofuels - II: Algal Biofuels and Microbial Fuel Cells.
URL <http://www.sciencedirect.com/science/article/pii/S0960852410011648>
7. Clavijo Rivera, E., Montalescot, V., Viau, M., Drouin, D., Bourseau, P., Frappart, M., Monteux, C., Couallier, E., 2018. Mechanical cell disruption of *parachlorella kessleri* microalgae: Impact on lipid fraction composition. *Bioresour. Technol.* 256, 77 – 85.
URL <http://www.sciencedirect.com/science/article/pii/S0960852418301706>

8. Clavijo, E., Villafaa Lpez, L., Liu, S., Bourseau, P., Frappart, M., Monteux, C., Couallier, E., 2017. Understanding microalgae lipids recovery by membrane processes: cross flow filtration of a representative synthetic mixture (o/w emulsion) (oral). In: 10th World Congress of Chemical Engineering (WCCE).
URL <https://hal.archives-ouvertes.fr/hal-1897689>
9. Delaunay, D., Rabiller-Baudry, M., Goálvez-Zafrilla, J. M., Balannec, B., Frappart, M., Paugam, L., 2008. Mapping of protein fouling by ftir-atr as experimental tool to study membrane fouling and fluid velocity profile in various geometries and validation by cfd simulation. *Chem. Eng. Process.* 47 (7), 1106 – 1117, euromembrane 2006.
URL <http://www.sciencedirect.com/science/article/pii/S025527010700390X>
10. Diagne, N. W., Rabiller-Baudry, M., Paugam, L., 2013. On the actual cleanability of polyethersulfone membrane fouled by proteins at critical or limiting flux. *J. Memb. Sci.* 425-426, 40–47.
URL www.sciencedirect.com/science/article/pii/S0376738812006667
11. Ding, L., Jaffrin, M. Y., 2014. Benefits of high shear rate dynamic nanofiltration and reverse osmosis: A review. *Sep. Sci. Technol.* 49 (13), 1953–1967.
URL [10.1080/01496395.2014.914538](https://doi.org/10.1080/01496395.2014.914538)
12. Du, X., Qu, F.-S., Liang, H., Li, K., Bai, L.-M., Li, G.-B., 2017. Control of submerged hollow fiber membrane fouling caused by fine particles in photocatalytic membrane reactors using bubbly flow: Shear stress and particle forces analysis. *Sep. Purif. Technol.* 172 (Supplement C), 130 – 139.
URL <http://www.sciencedirect.com/science/article/pii/S1383586616313399>
13. Flügel, E., 2010. *Microfacies of Carbonate Rocks. Analysis, Interpretation and A cation*, 2nd Edition. Springer
14. Frappart, M., Massè, A., Jaffrin, M. Y., Pruvost, J., Jaouen, P., 2011. Influence of hydrodynamics in tangential and dynamic ultrafiltration systems for microalgae separation. *Desalination* 265 (1-3), 279 – 283.
URL <http://www.sciencedirect.com/science/article/pii/S001191641000559X>
15. Goh, P., Lau, W., Othman, M., Ismail, A., 2018. Membrane fouling in desalination and its mitigation strategies. *Desalination*

425 (Supplement C), 130 – 155.

URL <http://www.sciencedirect.com/science/article/pii/S0011916417322300>

16. Halim, R., Danquah, M. K., Webley, P. A., 2012. Extraction of oil from microalgae for biodiesel production: A review. *Biotechnol. Adv.* 30 (3), 709 – 732.
URL <http://www.sciencedirect.com/science/article/pii/S0734975012000031>
17. Hong, A., Fane, A., Burford, R., 2003. Factors affecting membrane coalescence of stable oil-in-water emulsions. *J. Memb. Sci.* 222 (1-2), 19 – 39.
URL <http://www.sciencedirect.com/science/article/pii/S0376738803001376>
18. Hurt, E., Adams, M., Barbano, D., jun 2015. Microfiltration: Effect of channel diameter on limiting flux and serum protein removal1. *J. Dairy Sci.* 98 (6), 3599–3612.
URL <http://linkinghub.elsevier.com/retrieve/pii/S002203021500257X>
19. Hwang, K.-J., Wang, S.-Y., Iritani, E., Katagiri, N., 2016. Fine particle removal from seawater by using cross-flow and rotating-disk dynamic filtration. *J. Taiwan Inst. Chem. E.* 62, 45 – 53.
URL <http://www.sciencedirect.com/science/article/pii/S1876107016000699>
20. Jaffrin, M. Y., 2008. Dynamic shear-enhanced membrane filtration: A review of rotating disks, rotating membranes and vibrating systems. *J. Memb. Sci.* 324 (1-2), 7 – 25.
URL <http://www.sciencedirect.com/science/article/pii/S0376738808006182>
21. Jaffrin, M. Y., Ding, L.-H., Akoum, O., Brou, A., 2004. A hydrodynamic comparison between rotating disk and vibratory dynamic filtration systems. *J. Memb. Sci.* 242 (1-2), 155 – 167, membrane Engineering Special Issue.
URL <http://www.sciencedirect.com/science/article/pii/S0376738804003291>
22. Kumar Patel, A., Laroche, C., Marcati, A., Violeta Ursu, A., Jubeau, S., Marchal, L., Petit, E., Djelveh, G., Michaud, P., 2013. Separation and fractionation of exopolysaccharides from *porphyridium cruentum*.

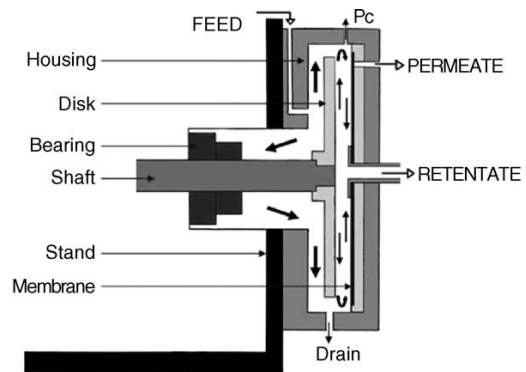
- Bioresour. Technol. 145, 345 – 350, special Issue: {IBS} 2012 & Special Issue: {IFIBiop}.
 URL <http://www.sciencedirect.com/science/article/pii/S0960852412018949>
23. 't Lam, G. P., Vermuë, M. H., Eppink, M. H. M., Wijffels, R. H., van den Berg, C., 2018. Multi-product microalgae biorefineries: From concept towards reality. *Trends Biotechnol.* 36, 216–227.
 URL <http://www.sciencedirect.com/science/article/pii/S0167779917302755>
 24. Lee, A. K., Lewis, D. M., Ashman, P. J., 2012. Disruption of microalgal cells for the extraction of lipids for biofuels: Processes and specific energy requirements. *Biomass Bioener.* 46, 89 – 101, international Conference on Lignocellulosic ethanol.
 URL <http://www.sciencedirect.com/science/article/pii/S0961953412002760>
 25. Li, L., Ding, L., Tu, Z., Wan, Y., Clause, D., Lanoisellé, J.-L., 2009. Recovery of linseed oil dispersed within an oil-in-water emulsion using hydrophilic membrane by rotating disk filtration system. *J. Memb. Sci.* 342 (1-2), 70 – 79.
 URL <http://www.sciencedirect.com/science/article/pii/S0376738809004657>
 26. Li, X., Příbyl, P., Bišová, K., Kawano, S., Cepák, V., Zachleder, V., Čížková, M., Brányiková, I., Vtová, M., 2013. The microalga *parachlorella kessleri*—a novel highly efficient lipid producer. *Biotechnol. Bioeng.* 110 (1), 97–107.
 URL [10.1002/bit.24595](https://doi.org/10.1002/bit.24595)
 27. Liu, S., Villafaa Lopez, L., Clavijo Rivera, E., Bourseau, P., Frappart, M., Couallier, E., 2018. Membrane filtration for the recovery of lipids from microalgae extracts (oral). In: *Euromembrane*.
 URL <https://hal.archives-ouvertes.fr/hal-01893857>
 28. Lorente, E., Hapońska, M., Clavero, E., Torras, C., Salvadó, J., 2017. Microalgae fractionation using steam explosion, dynamic and tangential cross-flow membrane filtration. *Bioresour. Technol.* 237 (Supplement C), 3 – 10
 29. Marcati, A., Ursu, Alina, V., Laroche, C., Soanen, N., Marchal, L., Jubeau, S., Djelveh, G., Michaud, P., 2014. Extraction and fractionation of polysaccharides and b-phycoerythrin from the

- microalga porphyridium cruentum by membrane technology. *Algal Res.* 5, 258 – 263.
URL <http://www.sciencedirect.com/science/article/pii/S2211926414000307>
30. Montalescot, V., Rinaldi, T., Touchard, R., Jubeau, S., Frappart, M., Jaouen, P., Bourseau, P., Marchal, L., 2015. Optimization of bead milling parameters for the cell disruption of microalgae: Process modeling and application to porphyridium cruentum and nannochloropsis oculata. *Bioresour. Technol.* 196, 339–346
 31. Moulai-Mostefa, N., Akoum, O., Nedjihoui, M., Ding, L., Jaffrin, M., 2007. Euromed 2006 comparison between rotating disk and vibratory membranes in the ultrafiltration of oil-in-water emulsions. *Desalination* 206 (1), 494–498.
URL <http://www.sciencedirect.com/science/article/pii/S0011916406014494>
 32. Ota, S., Oshima, K., Yamazaki, T., Kim, S., Yu, Z., Yoshihara, M., Takeda, K., Takeshita, T., Hirata, A., Bišová, K., Zachleder, V., Hattori, M., Kawano, S., 1 2016. Highly efficient lipid production in the green alga *parachlorella kessleri*: Draft genome and transcriptome endorsed by whole-cell 3d ultrastructure. *Biotechnol. Biofuels* 9 (1)
 33. Rios, S. D., Clavero, E., Salvadó, J., Farriol, X., Torras, C., 2011. Dynamic microfiltration in microalgae harvesting for biodiesel production. *Ind. Eng. Chem. Res.* 50 (4), 2455–2460.
URL [10.1021/ie101070q](https://doi.org/10.1021/ie101070q)
 34. Rossi, N., Jaouen, P., Legentilhomme, P., Petit, I., 2004. Harvesting of cyanobacterium *arthrospira platensis* using organic filtration membranes. *Food Bioprod. Process.* 82 (3), 244 – 250
 35. Rossignol, N., Vandanjon, L., Jaouen, P., Quéméneur, F., 1999. Membrane technology for the continuous separation microalgae/culture medium: compared performances of cross-flow microfiltration and ultrafiltration. *Aquacult. Eng.* 20 (3), 191 – 208.
URL <http://www.sciencedirect.com/science/article/pii/S0144860999000187>
 36. Safi, C., Liu, D. Z., Yap, B. H. J., Martin, G. J. O., Vaca-Garcia, C., Pontalier, P.-Y., 2014. A two-stage ultrafiltration process for separating multiple components of *tetraselmis suecica* after cell disruption. *J. Appl. Phycol.* 26 (6), 2379–2387.
URL [10.1007/s10811-014-0271-0](https://doi.org/10.1007/s10811-014-0271-0)

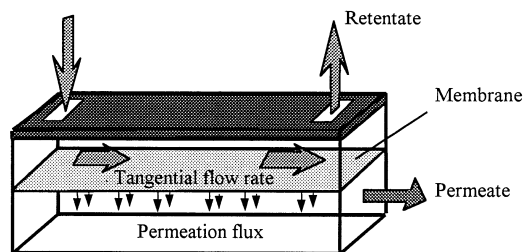
37. Świerczyńska, A., Bohdziewicz, J., Kamińska, G., Wojciechowski, K., 2016. Influence of the type of membrane-forming polymer on the membrane fouling. *Envir. Prot. Eng.* Vol. 42 (2), 197–210
38. Waghmare, A. G., Salve, M. K., LeBlanc, J. G., Arya, S. S., 2016. Concentration and characterization of microalgae proteins from *Chlorella pyrenoidosa*. *Bioresour. Bioprocess.* 16 (3).
URL <https://bioresources.bioprocessing.springeropen.com/articles/10.1186/s40643-016-0094-8>
39. Zhang, W., Ding, L., 2015. Investigation of membrane fouling mechanisms using blocking models in the case of shear-enhanced ultrafiltration. *Sep. Purif. Technol.* 141 (Supplement C), 160 – 169.
URL <http://www.sciencedirect.com/science/article/pii/S138358661400728X>
40. Zhao, F., Chu, H., Su, Y., Tan, X., Zhang, Y., Yang, L., Zhou, X., 2016. Microalgae harvesting by an axial vibration membrane: The mechanism of mitigating membrane fouling. *J. Memb. Sci.* 508 (Supplement C), 127 – 135.
URL <http://www.sciencedirect.com/science/article/pii/S0376738816300655>
41. Zinkone, T. R., Gifuni, I., Lavenant, L., Pruvost, J., Marchal, L., 2018. Bead milling disruption kinetics of microalgae: Process modeling, optimization and application to biomolecules recovery from *Chlorella sorokiniana*. *Bioresour. Technol.* 267, 458–465.
URL [10.1016/j.biortech.2018.07.080](https://doi.org/10.1016/j.biortech.2018.07.080)

Figure Captions

1	Filtration modules used in this study.	25
2	Flux (J) and normalized flux (J/J_w) of the model solution permeate versus TMP for the PAN 500 kDa and PVDF 0.4 μm membranes on the RD module with $\dot{\gamma}_{\text{max}}=66\,000\text{ s}^{-1}$. The error bars correspond to the standard deviation calculated from three independent measurements.	26
3	Evolution of the permeate flux (J) and its normalized representation (J/J_w) versus the VRR for the PAN 500 kDa and PVDF 0.4 μm membranes during the RD filtration ($\dot{\gamma}_{\text{max}}=66\,000\text{ s}^{-1}$). The error bars correspond to the uncertainty propagation from three independent measurements.	27
4	Normalized representation of the permeate flux versus the VRR with the 500 kDa PAN membrane at 30 $^{\circ}\text{C}$ during the RD and the CF filtrations. The error bars correspond to the uncertainty propagation from three independent measurements.	28
5	Volume droplet size distribution as a function of the VRR in the retentate sample using the 500 kDa PAN membrane for the CF and RD filtrations.	29
6	Normalized representation of the permeate flux of the supernatants, SN ₁ and SN ₂ , and the model solution (MS) versus the VRR with the 500 kDa PAN membrane and both filtration modules; RD module ($\dot{\gamma}_{\text{max}}=66\,000\text{ s}^{-1}$) and CF module ($\dot{\gamma}_{\text{max}}=16\,000\text{ s}^{-1}$) The error bars correspond to the uncertainty propagation from three independent measurements.	30

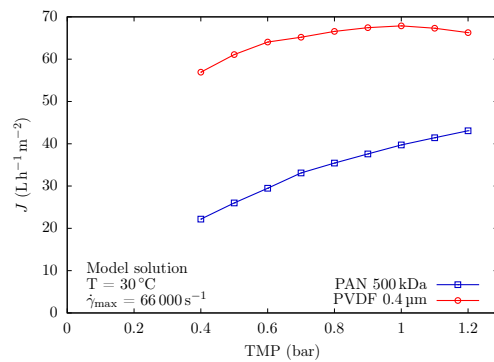


(a) Cross-sectional view of the rotating disk module (Frappart et al., 2006).

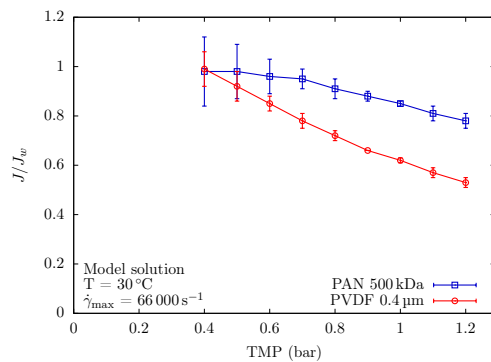


(b) Schematic of the crossflow module.

Figure 1: Filtration modules used in this study.

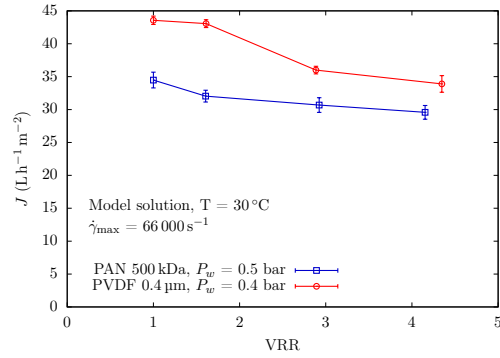


(a) Flux (J).

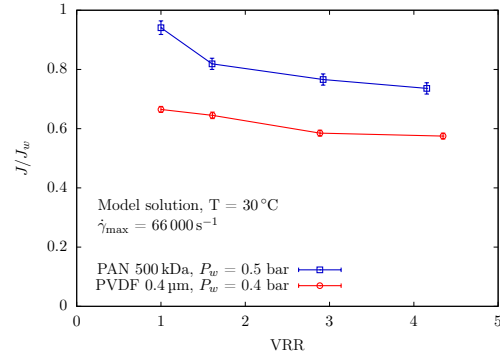


(b) Normalized flux (J/J_w).

Figure 2: Flux (J) and normalized flux (J/J_w) of the model solution permeate versus TMP for the PAN 500 kDa and PVDF 0.4 μm membranes on the RD module with $\dot{\gamma}_{\text{max}}=66\,000\text{ s}^{-1}$. The error bars correspond to the standard deviation calculated from three independent measurements.



(a) Flux (J).



(b) Normalized flux (J/J_w).

Figure 3: Evolution of the permeate flux (J) and its normalized representation (J/J_w) versus the VRR for the PAN 500 kDa and PVDF 0.4 μ m membranes during the RD filtration ($\dot{\gamma}_{\max}=66\,000\text{ s}^{-1}$). The error bars correspond to the uncertainty propagation from three independent measurements.

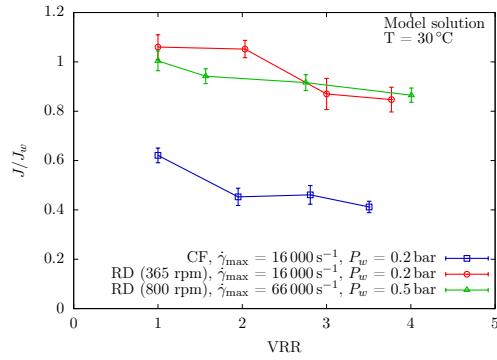
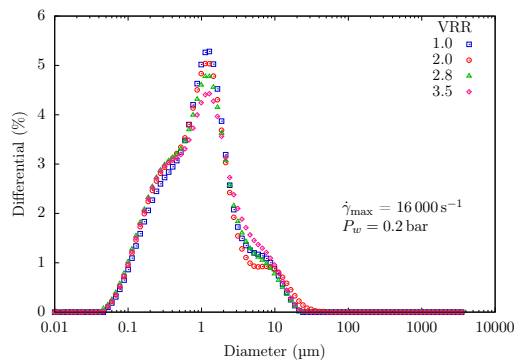
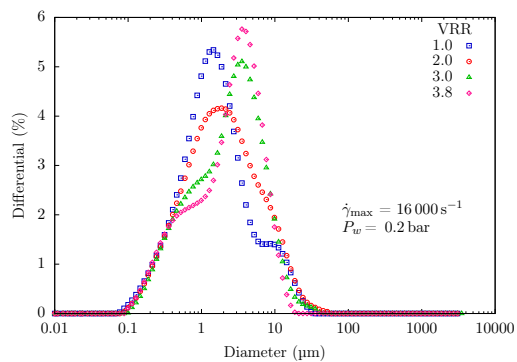


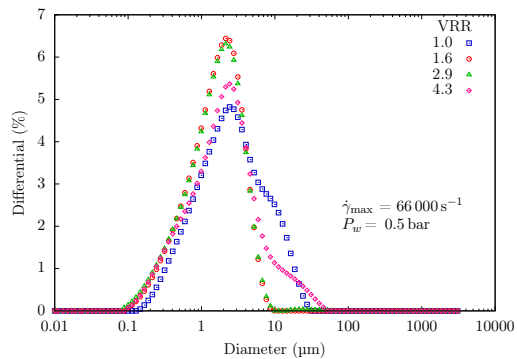
Figure 4: Normalized representation of the permeate flux versus the VRR with the 500 kDa PAN membrane at 30 °C during the RD and the CF filtrations. The error bars correspond to the uncertainty propagation from three independent measurements.



(a) Crossflow filtration.



(b) Rotating disk filtration at 365 rpm.



(c) Rotating disk filtration at 800 rpm.

Figure 5: Volume droplet size distribution as a function of the VRR in the retentate sample using the 500 kDa PAN membrane for the CF and RD filtrations.

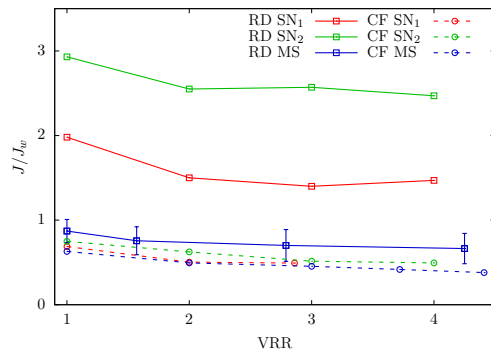


Figure 6: Normalized representation of the permeate flux of the supernatants, SN₁ and SN₂, and the model solution (MS) versus the VRR with the 500 kDa PAN membrane and both filtration modules; RD module ($\dot{\gamma}_{\max}=66\,000\text{ s}^{-1}$) and CF module ($\dot{\gamma}_{\max}=16\,000\text{ s}^{-1}$) The error bars correspond to the uncertainty propagation from three independent measurements.

Table Captions

1	Working parameters selected for both the RD and CF modules. Parameters for the RD module were obtained from Eq. (1), while Eq. (2) was used for the CF parameters.	32
2	J_w (1 bar), J_{lim} , P_{max} , J_c , and P_c values for the different membranes studied during the RD filtration with $\dot{\gamma}_{max} = 66\,000\text{ s}^{-1}$ at $30\text{ }^\circ\text{C}$. The standard deviation (σ) is calculated from three independent measurements.	33
3	% Flux decline, % FRR, q_{VRR}^{mb} , θ_w^0 , and θ_w^{VRR} at a VRR of 4.3 ± 0.1 , during the RD filtration at $\dot{\gamma}_{max} = 66\,000\text{ s}^{-1}$, and $30\text{ }^\circ\text{C}$. q_{VRR}^{mb} is reported with uncertainty propagation, while θ_w^0 and θ_w^{VRR} have standard deviations (σ) calculated from ten independent measurements.	34
4	v_{max} , $\dot{\gamma}_{max}$, J_{lim} , P_{max} , J_c , and P_c values for the 500 kDa PAN membrane at $30\text{ }^\circ\text{C}$ during the CF and the RD filtrations. The standard deviation (σ) is calculated from three independent measurements.	35
5	$\dot{\gamma}_{max}$, % Flux decline and q_{VRR}^{mb} (reported with uncertainty propagation) measured during the concentration experiment with the 500 kDa PAN membrane and both modules at the final average VRR = 3.8 ± 0.3 and $30\text{ }^\circ\text{C}$	36
6	Composition of the supernatants (SN ₁ and SN ₂) of bead-milled <i>Parachlorella kessleri</i> cultures before filtration, and composition of the retentates (RET ₁ and RET ₂) and permeates (PERM ₁ and PERM ₂) sampled at VRR=2 with the RD module at $\dot{\gamma}_{max} = 66\,000\text{ s}^{-1}$. The standard deviation (σ) was calculated from three independent measurements.	37

Table 1: Working parameters selected for both the RD and CF modules. Parameters for the RD module were obtained from Eq. (1), while Eq. (2) was used for the CF parameters.

Module	v_{\max} (m s^{-1})	$\dot{\gamma}_{\max}$ (s^{-1})
RD (365 rpm)	2.5	16000
RD (800 rpm)	5.4	66000
CF	2.0	16000

Table 2: J_w (1 bar), J_{lim} , P_{max} , J_c , and P_c values for the different membranes studied during the RD filtration with $\dot{\gamma}_{\text{max}} = 66\,000\text{ s}^{-1}$ at $30\text{ }^\circ\text{C}$. The standard deviation (σ) is calculated from three independent measurements.

Polymer	MWCO	$J_w \pm \sigma$ ($\text{L h}^{-1} \text{m}^{-2}$)	$J_{\text{lim}} \pm \sigma$ ($\text{L h}^{-1} \text{m}^{-2}$)	P_{max} (bar)	$J_c \pm \sigma$ ($\text{L h}^{-1} \text{m}^{-2}$)	P_c (bar)
PES	200 kDa	96 ± 2	62 ± 5	1.0	36 ± 4	< 0.4
PAN	500 kDa	75 ± 3	–	–	29 ± 8	0.5–0.6
PVDF	0.4 μm	123 ± 11	64 ± 20	0.6	57 ± 20	< 0.4
PVDF	1.5 μm	82 ± 8	65 ± 13	0.8	55 ± 13	0.5–0.6

Table 3: % Flux decline, % FRR, $q_{\text{VRR}}^{\text{mb}}$, θ_w^0 , and θ_w^{VRR} at a VRR of 4.3 ± 0.1 , during the RD filtration at $\dot{\gamma}_{\text{max}}=66\,000\text{ s}^{-1}$, and $30\text{ }^\circ\text{C}$. $q_{\text{VRR}}^{\text{mb}}$ is reported with uncertainty propagation, while θ_w^0 and θ_w^{VRR} have standard deviations (σ) calculated from ten independent measurements.

Polymer	MWCO	Flux decline (%)	FRR (%)	$q_{\text{VRR}}^{\text{mb}}$ (g m^{-2})	$\theta_w^0 \pm \sigma$ ($^\circ$)	$\theta_w^{\text{VRR}} \pm \sigma$ ($^\circ$)
PES	200 kDa	75–84	20	134 ± 19	79.4 ± 0.5	57.3 ± 0.6
PAN	500 kDa	14–40	100	378 ± 15	75.0 ± 2.4	69.2 ± 2.1
PVDF	0.4 μm	42–45	72	429 ± 18	95.1 ± 1.2	84.5 ± 0.5
PVDF	1.5 μm	23–85	47	6 ± 18	82.3 ± 0.7	80.6 ± 0.7

Table 4: v_{\max} , $\dot{\gamma}_{\max}$, J_{lim} , P_{\max} , J_c , and P_c values for the 500 kDa PAN membrane at 30 °C during the CF and the RD filtrations. The standard deviation (σ) is calculated from three independent measurements.

Module	v_{\max} (m s^{-1})	$\dot{\gamma}_{\max}$ (s^{-1})	$J_{\text{lim}} \pm \sigma$ ($\text{L h}^{-1} \text{m}^{-2}$)	P_{\max} (bar)	$J_c \pm \sigma$ ($\text{L h}^{-1} \text{m}^{-2}$)	P_c (bar)
CF	2.0	16000	19.7 ± 4.6	0.4	17 ± 2	0.2–0.3
RD (365 rpm)	2.5	16000	–	–	33 ± 6	0.3–0.4
RD (800 rpm)	5.4	66000	–	–	31 ± 3	0.5–0.6

Table 5: $\dot{\gamma}_{\max}$, % Flux decline and $q_{\text{VRR}}^{\text{mb}}$ (reported with uncertainty propagation) measured during the concentration experiment with the 500 kDa PAN membrane and both modules at the final average VRR = 3.8 ± 0.3 and 30 °C.

Filtration module	$\dot{\gamma}_{\max}$ (s^{-1})	Flux decline (%)	$q_{\text{VRR}}^{\text{mb}}$ (g m^{-2})
CF	16000	59	676 ± 231
RD (365 rpm)	16000	13	24 ± 23
RD (800 rpm)	66000	14	378 ± 15

Table 6: Composition of the supernatants (SN₁ and SN₂) of bead-milled *Parachlorella kessleri* cultures before filtration, and composition of the retentates (RET₁ and RET₂) and permeates (PERM₁ and PERM₂) sampled at VRR=2 with the RD module at $\dot{\gamma}_{\max}=66\,000\text{ s}^{-1}$. The standard deviation (σ) was calculated from three independent measurements.

	Dry matter (g L ⁻¹)	Lipids (g L ⁻¹)	Proteins (g L ⁻¹)	Sugar (g L ⁻¹)	Conductivity ($\mu\text{S cm}^{-1}$)	pH
SN ₁	2.00 ± 0.10	0.16 ± 0.02	0.38 ± 0.05	0.45 ± 0.04	1049 ± 8	7.6 ± 0.1
RET ₁	2.80 ± 0.05	0.33 ± 0.05	0.62 ± 0.01	0.42 ± 0.01	1231 ± 6	7.6 ± 0.1
PERM ₁	1.44 ± 0.09	0.00 ± 0.00	0.00 ± 0.02	0.22 ± 0.00	1092 ± 6	7.6 ± 0.1
SN ₂	1.34 ± 0.10	0.17 ± 0.03	0.19 ± 0.03	0.32 ± 0.07	993 ± 20	7.2 ± 0.1
RET ₂	1.76 ± 0.04	0.30 ± 0.03	0.23 ± 0.01	0.33 ± 0.01	1119 ± 6	7.3 ± 0.1
PERM ₂	1.00 ± 0.04	0.00 ± 0.00	0.05 ± 0.14	0.16 ± 0.02	947 ± 5	7.3 ± 0.1